Proceedings

APPLIED ELECTROMAGNETICS AND MECHANICS

Edited by

Phuong Ho-Thanh, Ha Ta-Hong, Ngan Huynh-Kieu, Chi Dang-Kim

The 7th Asia Pacific Symposium on Applied Electromagnetics and Mechanics

July 25-27, 2012, Ho Chi Minh city, Vietnam

JAPAN SOCIETY OF APPLIED ELECTROMAGNETICS AND MECHANICS

Enhance the Sensibility of the Eddy Current Testing

Hiroki KIKUCHIHARA[1], Iliana MARINOVA[2], Yoshifuru SAITO[1],
Manabu OHUCH[3], Hideo MOGI[3] and Yoshiro OIKAWA[3]

[1] Graduate School of Hosei University, Tokyo 184-8584, Japan
[2] Technical University of Sofia, Sofia 1756, Bulgaria
[3] Denshijiki Industry Co., Ltd, Tokyo 115-0051, Japan

Eddy current testing (ECT) is one of the most representative nondestructive testing methods for metallic materials, parts, structures and so on. Operating principle of ECT is based on the two major properties of magnetic field. One is that alternating magnetic field induces eddy current in all of the conducting materials. Thereby, an input impedance of the magnetic field source, i.e., electric source, depends on the eddy current path. Second is that the magnetic field distribution depends only on the exciting but also the reactive magnetic fields caused by the eddy currents in targets. Former and latter are the impedance sensing and magnetic flux sensing types, respectively.

This paper concerns with an improvement of sensibility of the impedance sensing method. Sensibility of the ECT is improved by means of two steps. One is an optimum exciting frequency selection. We employ the natural parallel resonant frequency of ECT coil. The other is to increase the sharpness of the resonance curve on impedance versus frequency characteristic by changing the coil connection. Thus, we have succeeded in developing the ECT sensor having up to 4 times higher sensibility compared with those of conventional one.

Key words: Eddy current, Nondestructive testing, Resonant frequency

1   Introduction

Modern engineering products such as air-plane, automobile, smart building, high speed train and so on are essentially composed of metallic materials for forming the shape of product, suspending the mechanical stress and constructing the structural frames. In particular, the mass transportation vehicles, e.g. large air plane, hi-speed train, express highway bus and so on, carrying a large number of people are required ultimately high safety as well as reliability.

To keep the safety of such vehicles, nondestructive testing to the metallic materials is one of the most important technologies because most of the structure materials are composed of the metallic materials.

Various nondestructive testing methods, such as eddy current testing (ECT), electric potential method, ultrasonic imaging and x-ray tomography, are currently used. Among these methods, ECT does not require complex electronic circuits and direct contact to target. Furthermore, target whose major frame parts are composed of conductive metallic materials can be selectively inspected by ECT [1,3].

Operating principle of ECT is very simple. The ECT is based on the two major properties of magnetic field. One is that exposing the conductive materials to the alternating magnetic fields induces eddy current in all of the conducting materials. Thereby, the input impedance of the magnetic field source, i.e., electric source, can detect the change of the target impedance caused by defects blocking eddy current flowing. The ECT based on this principle is called impedance sensing type. The other type utilizes a separately installed sensor coil to detect the leakage magnetic flux change. The magnetic field of ECT is composed of two components: one is the exciting and the other is the reactive magnetic fields. The reactive magnetic field is caused by the eddy currents in the target so that change of eddy current paths changes the reactive magnetic fields. Thus, the independently installed sensor detects this magnetic field change. This type is called a separately sensing coil type.

This paper concerns with an improvement of sensibility of the impedance sensing method. Improvement of the sensibility is carried out in the two major steps.

The first step is to select the optimum exciting frequency. We select the natural parallel resonant frequency of the ECT sensor coil when facing with a wholesome part of target. A system comprising the ECT facing with the wholesome part of target takes the maximum pure resistive impedance. When the ECT sensor coil meets with a defect of target, this resonance condition is essentially not satisfied. This makes it possible to maximize the deviation between the resonance and not resonance impedances.

The second step is to increase the resonant impedance as well as to sharpen the peaky impedance versus frequency characteristic by changing the coil connection [4]. Since the natural parallel resonance impedance become larger, then the deviation between the resonance and not resonance impedances is essentially larger. This essentially enhances the sensibility of ECT sensor.

2   Enhancement of ECT Sensibility

2.1 Operating principle of ECT

Let an arbitrary finite length solenoid coil shown in Fig. 1(a) be an eddy current sensor coil. When we put on this sensor coil on a copper plate as shown in Fig. 1(b) and apply an alternating current to the sensor coil, because of the Faraday's law, eddy current is induced as a reaction of the alternating magnetic fields. Measure the input impedance of the sensor coil is able to diagnose a difference of the target copper plate condition between no defects (Fig. 1(b)) and 2mm crack defect(Fig. 1(c)). This is similar to the secondary impedance change detection from primary input terminal in a conventional single phase transformer.

Thus, it is obvious that a simple finite length solenoid coil can detect the defects of the target conducting materials. This is the operating principle of ECT.


(a)Coil

(b)Copper plate with 1mm thickness

1 mm

(c)2mm Air-gap

2mm
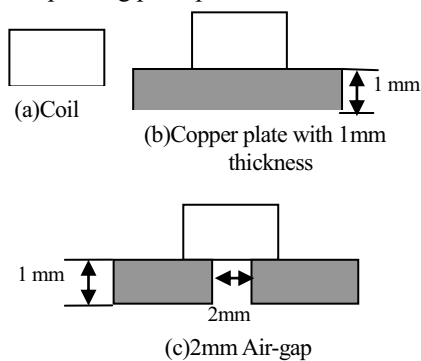
Fig.1 Tested coil and the measurement conditions.

2.2 Natural resonant phenomena of ECT coil

Any of the coils always exhibit an inductive property because of the magnetic fields around them by applying a current into the coil. However, any of the coils have the capacitances among the coils. Even though a simple finite length solenoid coil shown in Fig. 1(a), it is possible to observe its natural resonance phenomena as shown in Fig. 2. Figs 2(a) and 2(b) are the frequency f versus impedance |Z| and the frequency f versus phase ϕ characteristics, respectively.
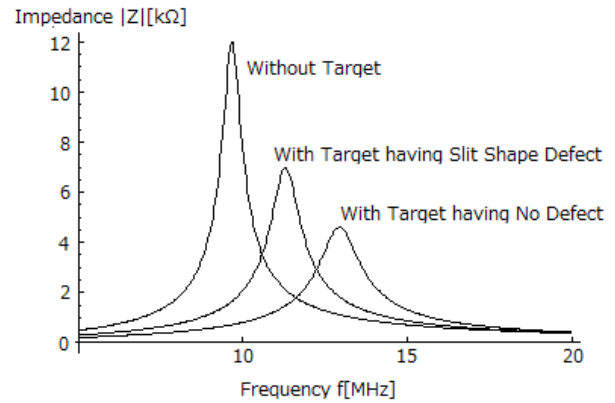
(a)   Impedance |Z| vs. Frequency f.
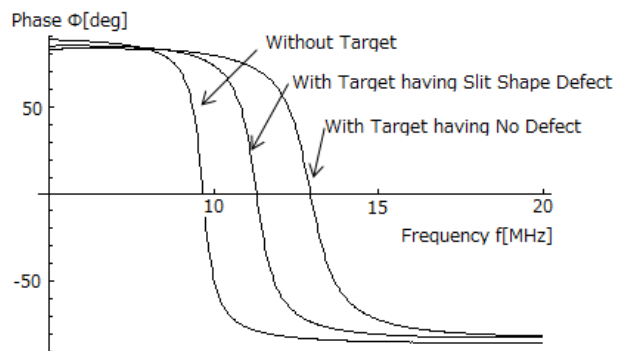
(b) Phase φ vs. Frequency f.

Fig.2   Frequency characteristics of the impedance and phase.

2.3 Optimum operation frequency

Decision of ECT operation frequency is of paramount importance, because sensibility and searching depth of ECT are greatly depending on the operation frequency. Theoretically, the operation frequency of ECT can be decided by taking the target conductivity and its skin-depth into account. However, final selection of operation frequency is determined by the past experiences and the practical tests.

In the present paper, we select the natural parallel resonant frequency of the ECT sensor coil when facing with a wholesome part of target. The ECT facing with the wholesome part of target takes the maximum pure resistive impedance. When the ECT sensor coil meets with a defect of target, the resonance condition is essentially not established. Therefore, the input impedance from sensor coil input terminals is also reduced to small in value compared with those of the resonant one. Namely, a deviation between the resonance and not resonance impedances becomes maximum value.

A sensibility ε of ECT is defined by

$$\varepsilon = \frac{|reference - measured|}{reference} \times 100[\%], \qquad (1)$$

where the reference and measured in (1) refer to the input impedances from the ECT coil terminals when facing the ECT coil with the wholesome and defect parts of target, respectively.

2.4 Enhancement of quality factor Q

The sensibility of (1) is greatly depended on the quality factor Q of the parallel resonance defined by

$$Q = \frac{f_0}{\Delta f}, \qquad (2)$$

where f_0 and Δf are the resonant frequency and the bandwidth, respectively.

The quality factor Q represents a sharpness of the resonant curve on the impedance versus frequency coordinate. So that high Q in (2) means high sensibility in (1).

To increase the quality factor Q, we employ the resonant connection shown in Fig. 3. Figs. 3(a) and 3(b) are the two

(a) Two conductors.

(b) Connection of the two conductors.

(c) Equivalent electric circuit of the connected conductors.

(d) Modified equivalent electric circuit of the connected conductors.
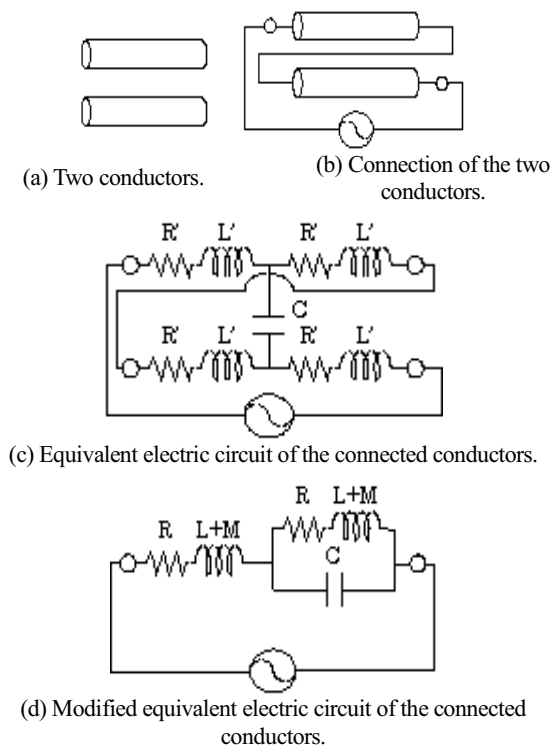
Fig.3   Principle of a resonance coil connection.

parallel conductors and their resonant connection, respectively. Denoting R, L, M as the resistance, self-inductance and, mutual inductance, it is possible to draw an equivalent circuit of the resonant connected two conductors as shown in Figs. 3(c), 3(d). Fig.4 shows a difference between the normal and resonant coil connection [4]. Practically, the resonant connection is carried out by twisting the two coils to uniform the facing side of both conductors as shown in Fig. 5 [5].


(a) Normal   (b) Resonance type
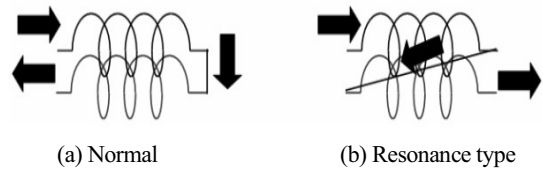
Fig.4   Comparison of the normal with resonant coil connections.

Fig. 5 Example of a pair of twisted coils

3 Experiment

3.1 Tested target peace and trial ECT coils

Fig. 6 shows a target peace which is composed of the two different types of materials (SUS304 and SUS316). A vertical line shape artificial crack having 10mm length, 0.2mm width and 0.5mm depth had been made to the sandwiched SUS by the electrical discharge machining. Fig. 6 shows a 20mm by 20mm target area. The ECT sensors measured at the 9 by 9 sampling points with 2.5mm regular spacing on this 20mm by 20mm square area.
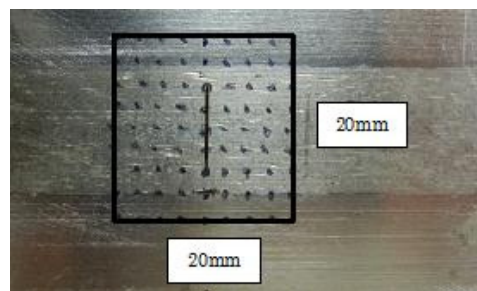

Fig. 6 Target test piece and measured points.
The test peace is composed of the two different types of SUS materials. A line shape artificial crack having 10mm length, 0.2mm width and 0.5mm depth had been made to the sandwiched SUS by the electrical discharge machining. A 20mm by 20mm square area is measured at the 9 by 9 points with 2.5mm regular spacing sampling

We have worked out a lots of ECT coils for comparison. Table 1 lists the representative 6 tested ECT coils. Every tested coil is wound around the Manganese-Zinc type ferrite bar used as an axial core material. No.1 is a normal ECT, No. 2 is a resonance type not employing twisting of coil, No.3 is a resonance type employing 100/m twisting, No.4 is a resonance type employing 150/m twisting, No.5 is a resonance type employing 200/m twisting, and No.6 is a resonance type employing 400/m twisting.

Table 1. Specification of the trial ECT coils.

No.1	Normal	Conductor length	50cm
		Diameter of conductor	0.1mm
		Axis core	Ferrite bar (MnZn)
		Coil outer diameter	2.4mm
		Coil inner diameter	2mm
		Coil length	6mm
		Number of twisted turns	0
		Number of coil layers	2
No.2	Resonant	Conductor length	50cm
		Diameter of conductor	0.1mm
		Axis	Ferrite bar (MnZn)
		Coil outer diameter	2.4mm
		Coil inner diameter	2mm
		Coil length	6mm
		Number of twisted turns	0
		Number of coil layers	2
No.3	Twisting	Conductor length	50cm
		Diameter of conductor	0.1mm
		Axis	Ferrite bar (MnZn)
		Coil outer diameter	3mm
		Coil inner diameter	2mm
		Coil length	5mm
		Number of twisted turns	100/m
		Number of coil layers	3
No.4	Twisting	Conductor length	50cm
		Diameter of conductor	0.1mm
		Axis	Ferrite bar (MnZn)
		Coil outer diameter	3mm
		Coil inner diameter	2mm
		Coil length	5mm
		Number of twisted turns	150/m
		Number of coil layers	3
No.5	Twisting	Conductor length	50cm
		Diameter of conductor	0.1mm
		Axis	Ferrite bar (MnZn)
		Coil outer diameter	3mm
		Coil inner diameter	2mm
		Coil length	5mm
		Number of twisted turns	200/m
		Number of coil layers	3
No.6	Twisting	Conductor length	50cm
		Diameter of conductor	0.1mm
		Axis	Ferrite bar (MnZn)
		Coil outer diameter	3mm
		Coil inner diameter	2mm
		Coil length	5mm
		Number of twisted turns	400/m
		Number of coil layers	3

3.2 Conventional ECT operating at 256kHz
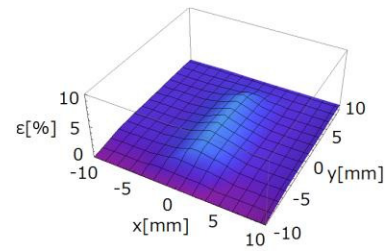
(a) No.1 Normal

(b) No.2 Resonant

(c) No.3 Twisting

(d) No.4 Twisting

(e) No.5 Twisting

(f) No.6 Twisting

Sensibility ε [%]
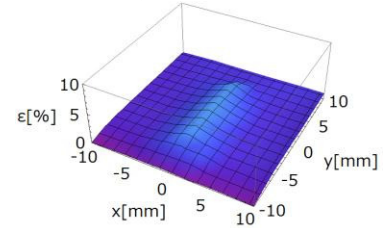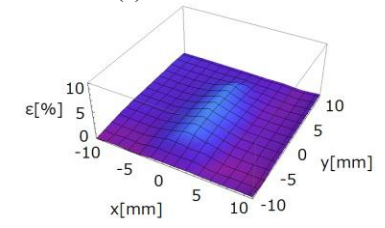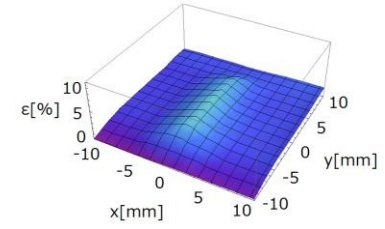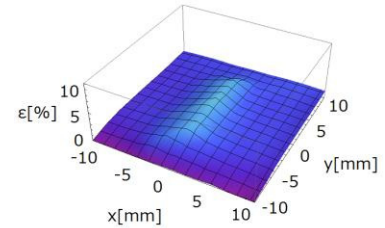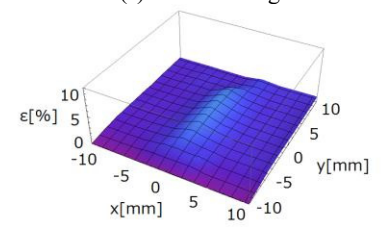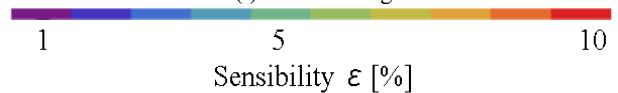
Fig. 7 Defect searching results. Any sensor coils can detect the two different kinds of base metallic materials.

At first, we evaluated the line shape crack in Fig. 6 by conventional ECT employing 256kHz operating frequency. Fig.7 shows the results of defect searching. Observe the results in Fig. 7 suggests that any of the sensor coils are capable of detecting the two different kinds of base metallic materials. Further, it is difficult to decide which sensor is the highest sensibility. In the other words, normal ECT defect searching using a particular operating frequency never reflects on the difference of the conductor connection and coil twisting.

3.3 ECT operating at resonant frequency

Any types of ECT coils have their own natural resonant frequency even if they are facing with the target without any defect. No.1,2,3,4,5 and 6 ECT coils in Table 1 have the natural resonant frequencies, 4650, 4950, 3650, 3300, 3425 and 3475 kHz, respectively. Fig. 8 shows the typical frequency characteristics of the trial ECT coils.
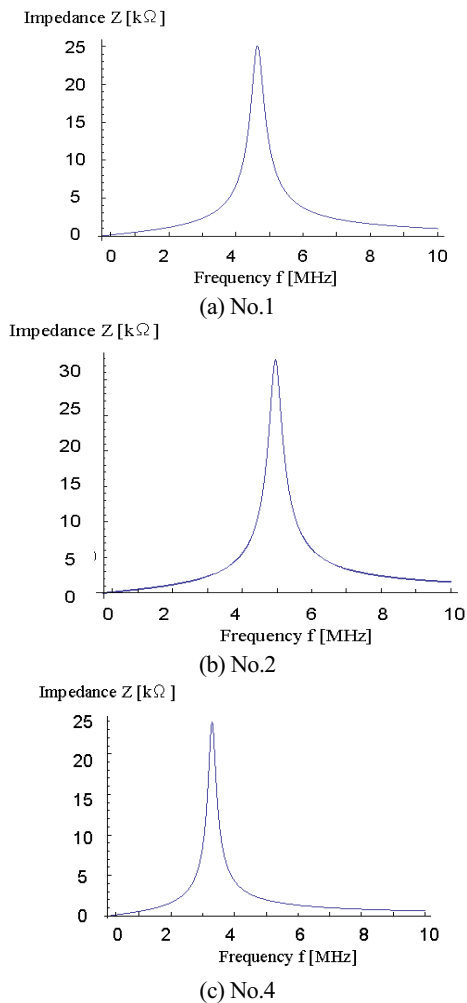
(a) No.1

(b) No.2

(c) No.4

Fig. 8 Frequency f vs. impedance $|Z|$ characteristics of the ECT coils (a) No.1, (b) No.2 and (c) No.4, respectively.

(a) No.1 Normal

(b) No.2 Resonant

(c) No.3 Twisting

(d) No.4 Twisting

(e) No.5 Twisting

(f) No.6 Twisting
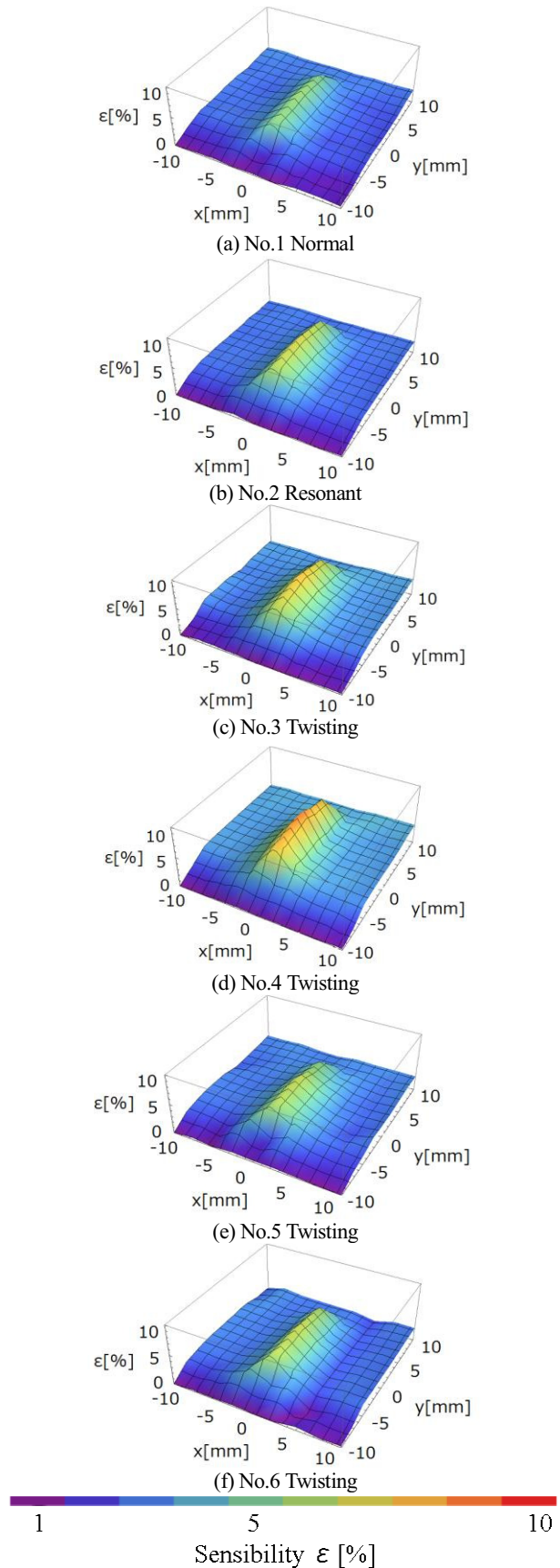
Fig. 9 The results of defect searching. Any sensor coils can detect two different kinds of base metallic materials.

Fig. 9 shows the defect searching result using each of the distinct natural resonant frequencies. Comparison of the results in Fig. 7 with that of Fig. 9 reveals that the resonant frequency operation is far superior sensibility in any ECT coils. In particular, No. 4 in Fig. 9(d) exhibits nearly 10% deviation. This fact is verified that the quality factor of No.4 in Fig. 9(b) is far excellent compared with those of   No.1 and of No.2.

Quality Factor Q

10.67

(a) No. 1

Quality Factor Q

14.05

(b) No.2

Quality Factor Q

14.40

(c) No.4
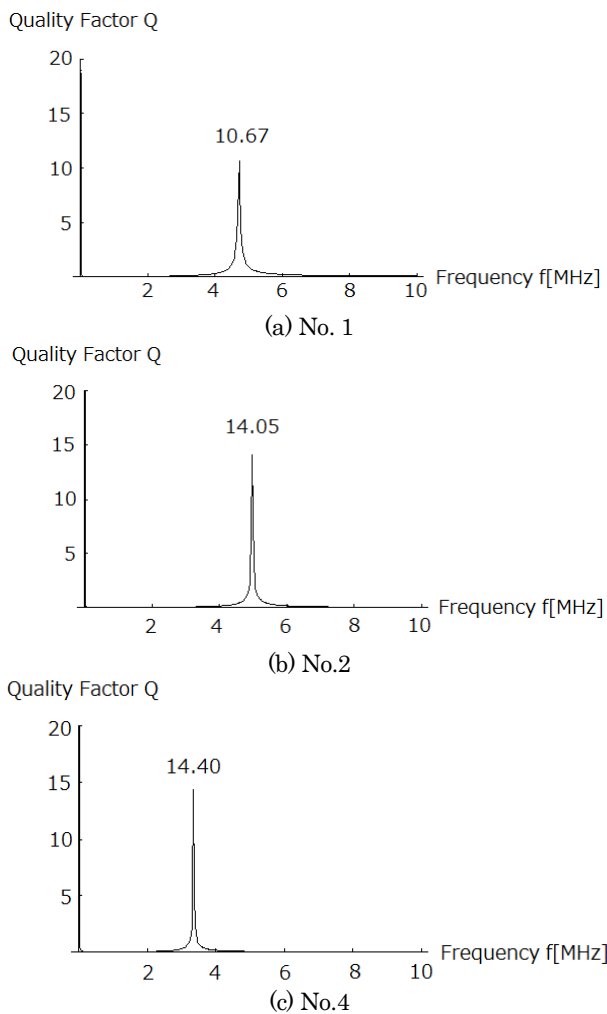
Fig. 10 Comparisons among the Quality Factor Q of the No.1,
No.2 and No,4 ECT coils.

4   Conclusion

New innovative idea to enhance the sensibility of ECT sensor has been proposed in this work. Our idea needs not any special tools but requires a consideration of natural resonance phenomena-, i.e., utilization of the resonant impedance, frequency and capacitive effect among the coils.

We have selected the natural parallel resonant frequency of the ECT sensor coil when facing with a wholesome part of target. When the ECT sensor coil has met with a defect of

target, the resonance condition has not been established. This has led that the impedance has reduced to small value compared with those at resonant condition. As a result, a deviation between the resonant and not resonant impedances has become the maximum. Thus, the sensibility of ECT sensor has been enhanced.

Further, connection of the conductors to be applied a half of the source voltage to adjacent conductors has made it possible to enhance the capacitive effect among the conductors.   Practically, this connection has been carried out by twisting the two coils to uniform the facing side of both conductors. Due to this enhancement of the capacitive effects, the resonant frequency has been reduced and succeeded in increasing the sensibility.

References

[1] I.Marinova, S.Hayano and Y.Saito, Ployphase eddy current testing, Journal of Applied Physics, Vol. 75, No.10, pp. 5904-5906, 1994.

[2] N.Burais and A.Nicolas, Electromagnetic field analysis in remote field eddy current testing systems, IEEE Transactions on Magnetics, Vol.25, No.4, pp.3010-3012, 1989.

[3] S.McFee and J.P.Webb, Automatic mesh generation for h-p adaption, IEEE Transactions on Magnetics, Vol.29, No.2, pp.1894-1897, 1993.

[4] Y.Midorikawa, S.Hayano and Y.Saito, A resonant phenomenon between adjacent series connected coils and its application to a als, Advanced Computational and Design Techniques in Applied Electromagnetic Systems, Vol.6, pp. 633-639, 1995.

[5] S.Hayano, Y.Nakajima, H.Saotome and Y.Saito, A new type high frequency transformer, IEEE Transactions on Magnetics, Vol. 27, No.6, pp.5205-5207, 1991.

Fluctuation Frequency Analysis of the Barkhausen Signals

Jun KAWAZOE[*1], Iliana Marinova[*2] and Yoshifuru SAITO[*1]

[*1] Graduate School of Hosei University, Tokyo 184-8584, Japan

[*2] Technical University of Sofia, Sofia 1756, Bulgaria

Ferromagnetic materials are widely used for various artificial products such as cars, trains, ships and so on. Because of its mechanical property, iron steel is most popular in use for the frame materials. Nondestructive testing of iron steel is an extremely important way to maintain their mechanical reliability. As is well known fact that the Barkhausen signals are emitted from only the ferromagnetic materials having magnetic domain structures. Also this signal varies depending upon their past mechanical as well as radioactive stress histories.

In the present paper, we have applied a generalized frequency fluctuation analysis to the Barkhausen signals to detect the various mechanical stresses. Surprisingly, it has been succeeded in clarifying that application of our frequency fluctuation analysis to the Barkhausen signals makes it possible to detect the several kinds of mechanical stress.

Key words: Barkhausen signal, Frequency fluctuation, Signal processing, Least squares

1. Introduction

Barkhausen signal is popularly observed in the ferromagnetic materials composed of the magnetic domain structures, e.g. iron, nickel, cobalt and garnet, when they are magnetizing. Also, it is well known that the Barkhausen signals are very sensitive to the physical external input, such as mechanical stress and radioactive damage, to the ferromagnetic materials.

The iron and its composite ferromagnetic materials are widely used for main frame materials to support the mechanical structures in many artificial products and constructions. Because of their essential role, they are always got mechanical stress and they keep their past mechanical stress histories. Nondestructive detection of their mechanical stress as well as residual stress is of paramount importance for keeping the safety of the mechanical structures, since it is possible to see ahead of time what extent the mechanical structure will maintain their strength for further use.

According to the past researches concerning to a relationship between the Barkhausen signal and applied mechanical stress, it has been revealed that Barkhausen signals are very sensitive to the mechanical stress and radioactive damage but any deterministic regularity has not been found [1,2].

Recently, only a macroscopic regularity has been reported by means of a frequency fluctuation analysis approach [3]. Principal purpose of this paper is that conventional frequency fluctuation analysis employing only 1st order fluctuation is generalized to the frequency fluctuation analysis employing the nth order fluctuations.

As a result, we succeed in extracting the distinct difference between the stressed and not stressed Barkhausen signals. Also, we succeed in visualizing in a most clear manner on the four dimensional space, whose coordinates are composed of the terms representing the higher order frequency fluctuation terms of Barkhausen signals.

One of the most famous frequency fluctuations is the 1/f frequency fluctuation, which can be observed in most of the natural phenomena such as natural wind, sea water waves, river flow sound and so on gives a healing effect to the mentalities via human sensibilities[4].

Conventional 1/f frequency analysis is that application of the 1st order least squares to the both Fourier power spectrum and frequency extracts the 1st order frequency fluctuation, i.e., Log of Fourier power spectrum is approximated by Log of $a_0 + a_1 f$, yields a 1st order frequency fluctuation characteristic, where a_0 and a_1 are the 0th and a 1st order frequency fluctuation terms, respectively. If the frequency fluctuation term a_1 takes $a_1=1$, then we have the 1/f frequency fluctuation.

On the other side, we generalize this conventional 1st order frequency fluctuation to the nth order frequency fluctuation characteristics, i.e., Log of Fourier power spectrum is approximated by a Log of $a_0 + a_1 f + a_2 f^2 + ... + a_n f^n$, where $a_0, a_1, a_2,..., a_n$ are the $0^{th}, 1^{st} 2^{nd}, ... , n^{th}$ order frequency fluctuation terms, respectively. Careful examination of the coefficients $a_0, a_1, a_2,..., a_n$ leads to the precise frequency fluctuation characteristic of the Barkhausen signal.

Second important key point of our approach is how to visualize the dependency of the $0^{th}, 1^{st}, 2^{nd}, ... , n^{th}$ order frequency fluctuation terms to the externally applied forces.

According to our experimental results on this research, most of the frequency fluctuation characteristics are sufficiently represented up to the 4th order terms. So that let the normalized $1^{st}, 2^{nd}, 3^{rd}, 4^{th}$ order frequency fluctuation coefficients be respectively the coordinate values on the x-, y-, z-axes, and point color, then up to the 4th order frequency fluctuation characteristics locate the three dimensional space coordinate position and point color. Thus, comparison among the different specimens of this diagram visualizes an each of the distinct characteristics depending on their mechanical stress conditions.

2. Frequency Fluctuation Analysis

2.1 Basic equations

Let us consider an arbitrary signal $g(t)$ and its Fourier power spectrum $G(f)$, and take the logarithm of both Fourier Spectrum $G(f)$ and frequency f. Plot the $\log G(t)$ on the $\log f$ coordinate represents a frequency characteristic of the signal $g(t)$ on the frequency domain, i.e., the frequency characteristic of the original signal is represented on a x-y plane coordinate system whose horizontal x- and vertical y-axes are corresponding to the logarithms of Fourier power spectrum $G(f)$ and of frequency f, respectively.

In order to represent a global frequency characteristic of the original signal $g(t)$ in frequency domain, apply a following power series function:

$$h(f) = a_0 + a_1 f + a_2 f^2 + \ldots + a_n f^n, \quad (1)$$

in this x-y plane makes it possible to evaluate the higher order frequency fluctuation analysis.

The coefficients $a_0, a_1 a_2, \ldots, a_n$ in (1) are determined by least squares as

$$\mathbf{A} = \left[C^T C \right]^{-1} \mathbf{C}^T \mathbf{Y}, \quad (2)$$

where a superscript T denotes a matrix transpose; the vectors $\mathbf{A}$, $\mathbf{Y}$ and matrix C are respectively given by

$$\mathbf{A} = \begin{bmatrix} a_0 & a_1 & . & a_n \end{bmatrix}^T, \quad (3)$$

$$\mathbf{Y} = \begin{bmatrix} h(f_0) & h(f_1) & . & h(f_m) \end{bmatrix}^T, \quad (4)$$

$$C = \begin{bmatrix} 1 & f_0 & f_0^2 & . & f_0^n \\ 1 & f_1 & f_1^2 & . & f_1^n \\ 1 & f_2 & f_2^2 & . & f_2^n \\ . & . & . & . & . \\ 1 & f_m & f_m^2 & . & f_m^n \end{bmatrix}, \quad (5)$$

$m > n$.

In (3)-(5), a number of equations m, i.e. number of the sampled frequencies $f_0, f_1 f_2, \ldots, f_n$, always greater than those of unknowns n, i.e., number of the coefficients $a_0, a_1 a_2, \ldots, a_n$. In most case, this condition is satisfied because of the number of sampled frequency m is much greater than those of the order n of the function $h(f)$ in (1).

2.2 Classical 1st order frequency fluctuation

Fig. 1 shows a Barkhausen signal measurement devices.
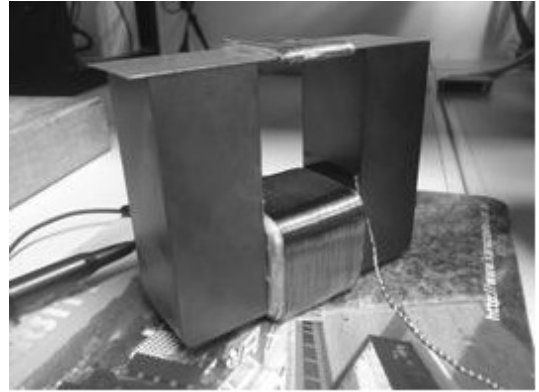
Fig.1.   Barkhausen signal measurement devices.

The tested specimens are the silicon steels with the 0.35mm thickness, 30mm width and 100mm length. The tested specimen is put on the upper two head surfaces of U shape ferrite core wound the 300 turns exciting coil. The specimen in Fig.1 is excited by flowing a 1A sinusoidal alternating current through this exciting coil.

Fig. 2 shows a typical frequency characteristic of a Barkhausen signal under no stress.
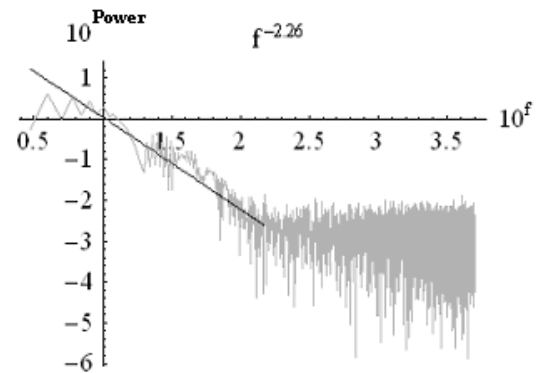

Fig. 2.   An example of typical frequency characteristic of a Barkhausen signal under no stress.

The frequency characteristic in Fig. 2 is obviously divided into two frequency regions. One is lower frequency region whose frequency fluctuation can be approximated by $f^{2.26}$ derived from 1st order approximation in (1), and the other higher one is a dispersing signal whose frequency fluctuation can be approximated by f^0, i.e. white noise.

On the other side, Fig. 3 show a typical frequency characteristic of Barkhausen signal under 3kg stressed.
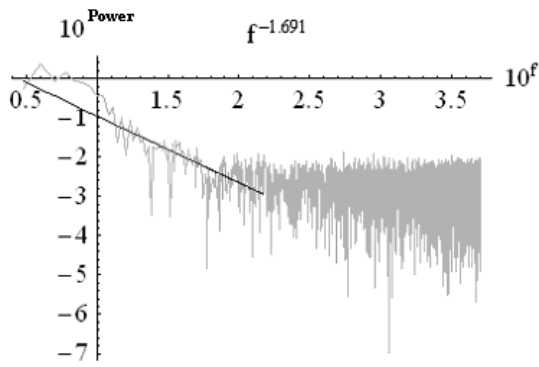
Fig. 3. An example of typical frequency characteristic of a Barkhausen signal under 3kg stressed.

The frequency characteristic in Fig. 3 is also divided into the two frequency regions. One is lower frequency region whose 1st order frequency fluctuation can be approximated by $f^{1.69}$, and the other higher one is a dispersing signal whose frequency fluctuation can be approximated by f^0.

Consideration to the difference between the first order frequency fluctuations $f^{2.26}$ and $f^{1.69}$ suggests that an application of the 3kg stress to the tested silicon steel changes the steep 1st order gradient -2.26 to the smoothly gradient -1.68. This result had been verified by the 1st order frequency fluctuation analysis to the 30 distinct sample specimens [3].

Thus, it is possible to detect the stress on the ferromagnetic materials by the classical 1st order frequency fluctuation analysis [3].

However, several difficulties are still remaining: One is how to decide the frequency range to be computed the frequency fluctuation characteristic. Second is that the 1st order frequency fluctuation analysis is only effective to a relatively large stress, even though it is required to detect the much more smaller stresses.

2.3 Generalized frequency fluctuation

Fig. 4 shows a frequency fluctuation characteristic under no stress along with a curve obtained by up to the 4th order power series function in (1), where the frequency sampling points have been taken in a logarithmic order.

To check the reproducibility of the coefficients a_1, a_2, a_3, a_4 , we have 10~12 times independently measured and computed these coefficients a_1, a_2, a_3, a_4 in (1) to the same specimen.
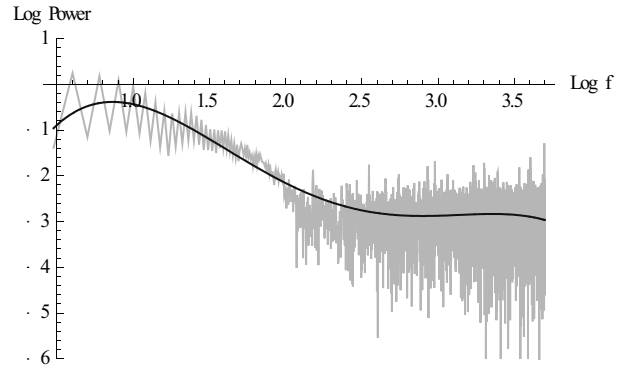

Fig. 4. Example of typical frequency characteristic of a Barkhausen signal under no stress along with an up to 4th order power series curve in (1).

After normalizing all of the coefficients a_1, a_2, a_3, a_4 to be the values between 1 and 0, let the normalized coefficients a_1', a_2', a_3', a_4' be respectively corresponded to the x-, y-, z-axes values and point color, then this makes it possible to visualize a dispersion characteristic of the coefficients a_1', a_2', a_3', a_4' . Fig. 5 shows a dispersion characteristic of these coefficients a_1', a_2', a_3', a_4' . Combination of Figs. 5(a) with 5(b) reveals that the dispersion is limited along the vicinity of a hatched surface in Fig. 6.
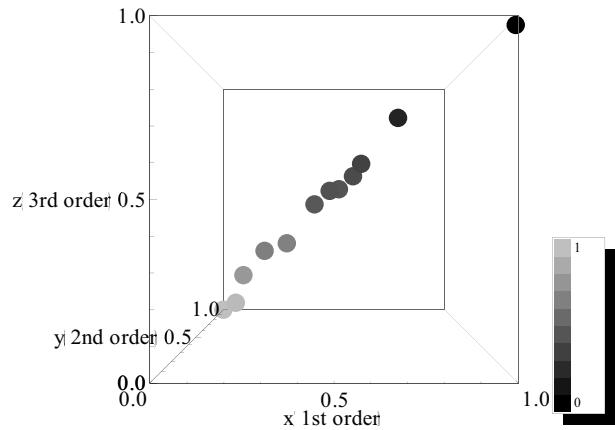
(a) x-y plane
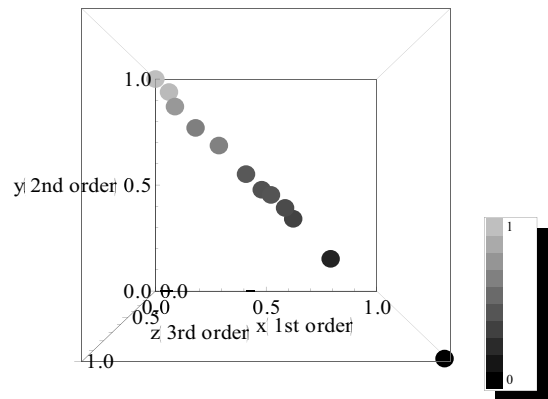
(b) x-z plane

Fig.5. Dispersion of the frequency fluctuation coefficients.
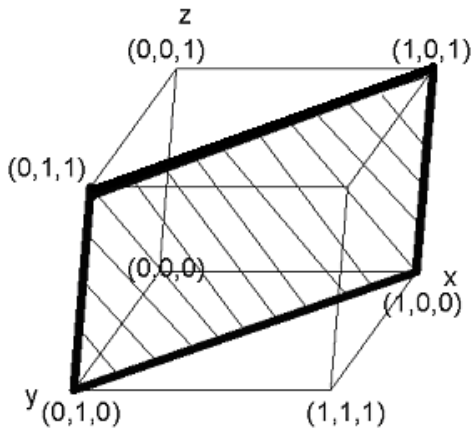
Fig.6. The normalized frequency fluctuation coefficients a_1', a_2', a_3', a_4' dispersing area (hatched surface).

Consideration to the hatched region in Fig. 6 suggests that an individual difference among the sound silicon steel without any stresses could be limited along the vicinity of the hatched surface in Fig. 6.

2.4 Stress visualization

We have carried out the random stresses visualization in much the same as described in Section 2.3. These stresses were applied to the specimen by hanging the random weights by a string as shown Fig. 7.
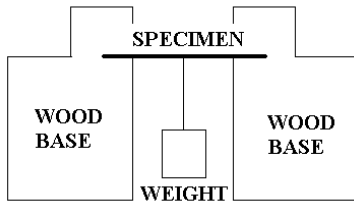
Fig.7. The stresses are applied by hanging the weights.

Fig. 8 shows one of the frequency fluctuation characteristics under stress along with a curve obtained by the *4th* order power series function in (1).
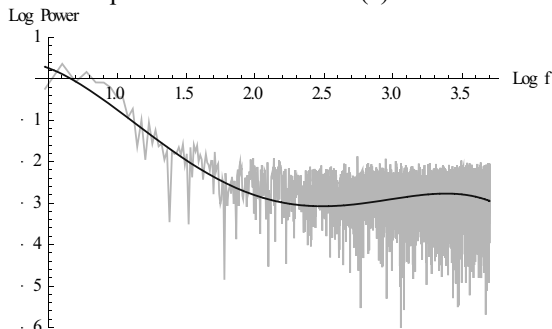
Fig. 8. One of the frequency characteristic of the Barkhausen signals under stress along with the *4ᵗʰ* order power series curve in (1).

Fig. 9 shows the dispersion characteristics of coefficients a_1', a_2', a_3', a_4'.

Comparison of the dispersion characteristics in Fig. 5(a) with that of Fig. 9(a) demonstrates a distinct effect of the applied stress. Also, comparison of the dispersion characteristics a_1', a_2', a_3', a_4' in Fig. 5(b) with that of Fig. 9(b) suggests the same as before.

Combination of Figs. 9(a) and 9(b) yields the results shown in Figs. 10 and 11.

(a) x-y plane

(b) x-z plane
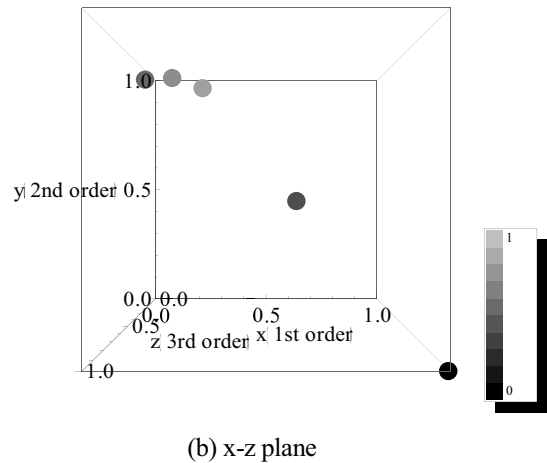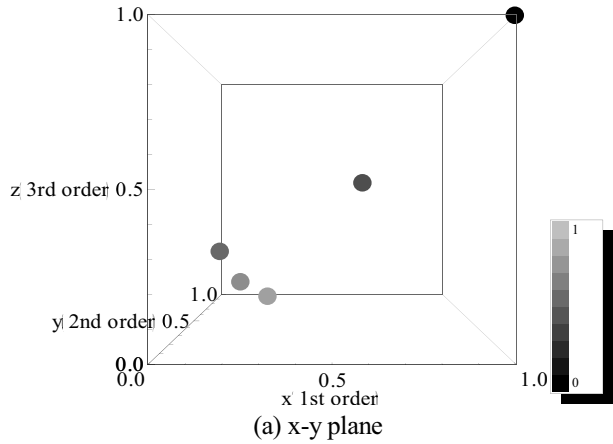
Fig.9. Dispersion of the frequency fluctuation coefficients.
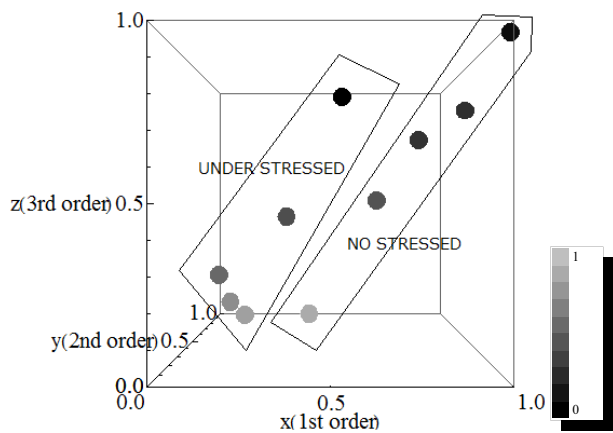
Fig. 10. The normalized frequency fluctuation coefficients a_1', a_2', a_3', a_4' difference between the stressed and no stressed groups on the x-y plane.
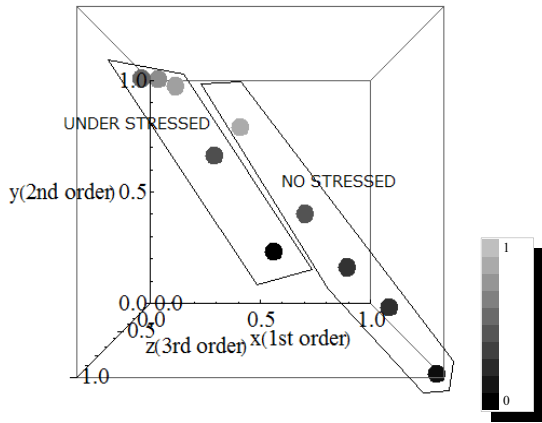
Fig. 11.   The normalized frequency fluctuation coefficients a_1', a_2', a_3', a_4' difference between the stressed and no stressed groups on the x-z plane.

Observation of the dispersion characteristics of the stressed specimens suggests that the normalized coefficients a_1', a_2', a_3', a_4' in (1) do not disperse but focus on a relatively small area. On the contrary, the normalized coefficients a_1', a_2', a_3', a_4' in (1) of the stress free specimens disperse the vicinity of hatched area in Fig. 6. This means that the externally applied stress suppresses the dispersion and confines them into the small space in Fig. 6.

2.5 Bending effect visualization

We have carried out the bending effect visualization in much the same as described in Section 2.4.

As shown the bended examples in Fig. 12, the 4 specimens were bended 0, 5, 15, and 45 degree. After that these 4 specimens were recovered to the original straight form.
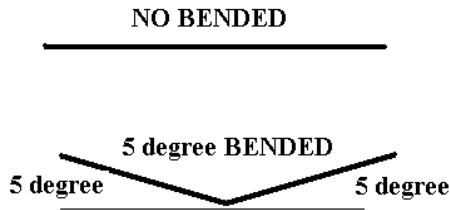

Fig. 12.   No bended and 5 degree bended.

Fig. 13 shows one of the frequency fluctuation characteristics after bending along with a curve obtained by the 4th order power series function in (1).
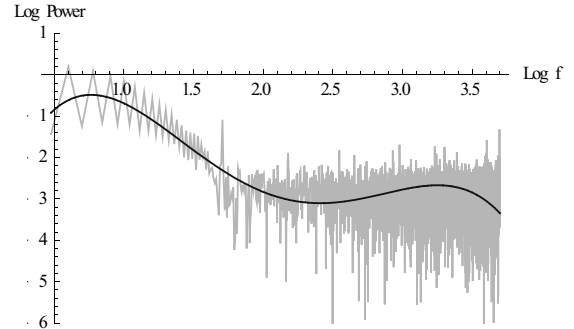

Fig. 13.   One of the frequency characteristics of the Barkhausen signal after bending a specimen along with the 4th order power series curve in (1).
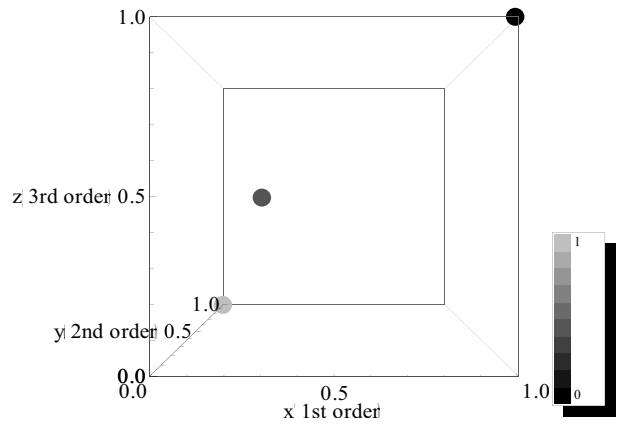
(a) x-y plane
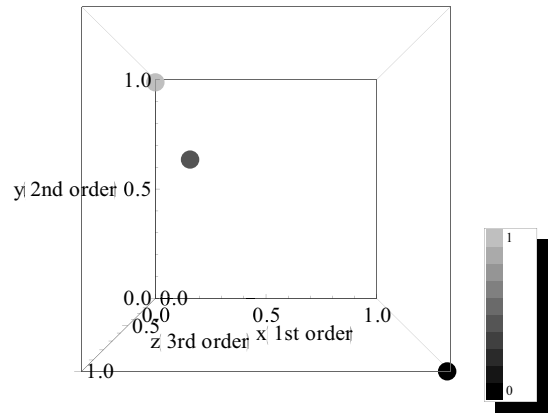
(b) x-z plane

Fig.14.   Dispersion of the frequency fluctuation coefficients.

Fig. 14 shows the normalized dispersion characteristics of coefficients a_1', a_2', a_3', a_4'.

Comparison of the dispersion characteristics in Fig. 5(a) with that of Fig. 14(a) demonstrates a distinct effect of the bending. Also, comparison of the dispersion characteristics in Fig. 5(b) with that of Fig. 14(b) suggests the same as before.
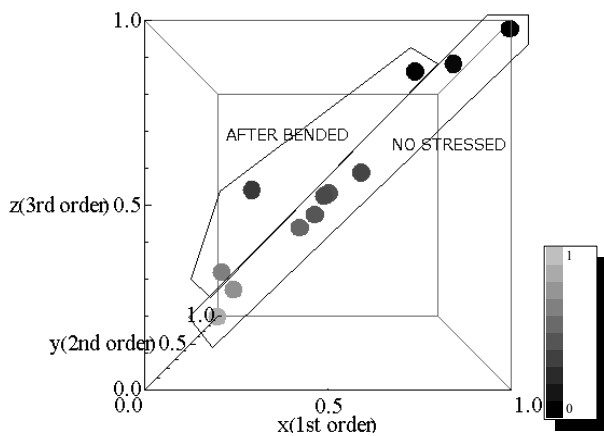
Fig. 15.   The normalized frequency fluctuation coefficients a_1', a_2', a_3', a_4' difference between the bending and not bending groups on the x-y plane.
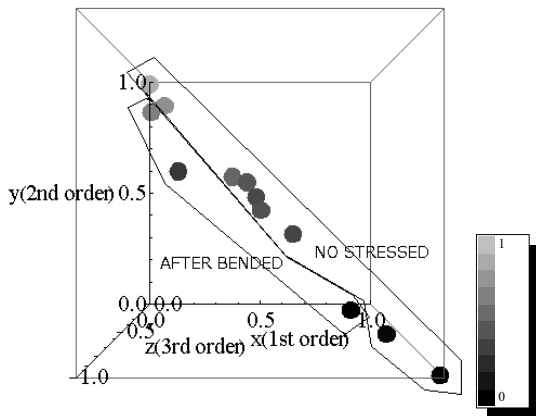

Fig. 16.   The normalized frequency fluctuation coefficients a_1', a_2', a_3', a_4' difference between the bending and not bending groups on the x-z plane.

Combination of Figs. 14(a) and 14(b) yields the results shown in Figs. 15 and 16.

Observation of the dispersion characteristics of the bended specimens suggests that the normalized coefficients a_1', a_2', a_3', a_4' in (1) do not disperse but focus on a relatively small area. On the other side, the normalized coefficients a_1', a_2', a_3', a_4' in (1) of the bended free specimens disperse the vicinity of the hatched surface in Fig. 6. Thereby, the externally applied bending stress suppresses this dispersion and confines them into the small space in Fig. 6.

Thus, it is obvious that the distinction between the stressed and bending effects is difficult from the Barkhausen signal analysis.

3. conclusion

Previously, we have succeeded in detect the applied stress on the silicon steel by means of the frequency fluctuation method [3].

This paper has generalized this approach, i.e., *1st* order to the *nth* order frequency fluctuations. Further, the *4th* order

frequency fluctuation characteristics could be visualized in a three dimensional space. This has clarified each of the distinct differences among the specimen having the same specifications, also clarified the measurement data dispersions.

As the concrete examples, we have applied our method to the stress visualization of the silicon steels, and succeeded in extracting the characteristics of the stressed specimens. Also, we have applied our method to the past bended history detection. This has led to the similar results obtained in the stress detection. Thereby, it has been clarified that the distinct difference between the past stressed or bended histories is difficult.

References

[1]   R M. Bozorth: Ferromagnetism, p. 462 (IEEE PRESS)

[2]   M. Katsumata, S. Hayano and Y. Saito: A Study of Barkhausen Phenomenon Visualization, *The Visualization Society of Japan*, B203, July (2003).

[3]   S. Nojima and Y. Saito: Application of Frequency Fluctuation to Barkhausen Signals and its Application, J. Magn. Soc. Jpn., 35, 380-385 (2011).

[4]   M. Teranishi, K. Maruyama, S. Hayano, and Y. Saito: Visualization of 1/f Frequency Component in Dynamic Image of Natural Phenomena, *The Visualization Society of Japan*, B108, July (2005).